Toyohisa Kaneko
IBM Federal Systems Division
Houston, TX 77058

Evaluation of LANDSAT Image Registration Accuracy

An algorithm determined that registration errors of LANDSAT imagery used for the Large Area Crop Inventory Experiment was 1.0 pixel.

Introduction and Problem Statement

An algorithm was developed to check image registration results in the Large Area Crop Inventory Experiment (LACIE). The LACIE project has been undertaken jointly by the U. S. Department of Agriculture, the National Oceanic and Atmosphere Administration (NOAA), and the National Aeronautics and Space Administration (NASA). The objective of this experiment is to demonstrate the capability to forecast the annual production of major crops such as wheat and corn, based upon image data from LANDSAT and meteorological data from the NOAA satellites and ground stations. The initial objective is focused on wheat. The details of this experiment are described by MacDonald *et al.*[1]

Abstract: *The Large Area Crop Inventory Experiment (LACIE) is an attempt to demonstrate the capability to forecast the annual production of major crops such as wheat and corn. Good image registration of data acquired on different dates is one of the key assumptions made in LACIE. This paper describes an algorithm to measure the accuracy of the current registration procedure. This algorithm employs a modified version of sequential similarity detection algorithm (SSDA). Based on over 264 registration checks, it was found that the root-mean-square of registration errors was 1.0 pixel. The failure rate of our registration checking algorithm was less than 10 per cent and the standard deviation of the accuracy of this algorithm was less than 0.2 picture element.*

The basic sample unit or segment in LACIE is a so-called LACIE image. These images are 196 picture elements (pixels) by 117 scan lines for each of four channels*. There are about 2,000 sample segments in the United States, on each of which the acreage of wheat must be estimated. These segments are extracted from full frame LANDSAT images. A full frame LANDSAT image covers an area approximately 180-by-180 km on the ground, whereas a LACIE image covers an area of 8-by-10 km. To classify wheat from non-wheat, up to four acquisitions of imagery representing four different biological phases of wheat growth are taken. These four channel images are merged into a multi-temporal image. The resulting number of channels is $4N$ where N is the number of acquisitions. The current classification method is a sum-of-likelihoods classifier[1,2]. With this classification scheme, it is assumed that imagery from different acquisitions has been spatially aligned or registered. If misregistration occurs, a pixel value takes the value of its neighboring point in the misregistered channels, which could be from a different crop.

* Channel 1 of the multi-spectral scanner (MSS) is in the wavelength of 0.5 to 0.6 μm, channel 2:0.6 to 0.7, channel 3:0.7 to 0.8, and channel 4:0.8 to 1.1.

Photogrammetric Engineering and Remote Sensing,
Vol. 42, No. 10, October 1976, pp. 1285-1299

The first step of registration is to locate a sample segment on the 185-by-185-km LANDSAT image based upon the best estimate of the position and attitude of LANDSAT gathered through one or more ground stations. These data can predict the satellite's multispectral scanner field-of-view with a standard deviation of 4.5 km in the location on the earth's surface. To guarantee the successful inclusion of a 9-by-11-km sample segment, a search area of 18-by-20 km (354 pixels-by-234 scan lines) is selected from a LANDSAT frame. Then a procedure called resampling is carried out to correct known geometrical errors caused by satellite height variation and rotation. The final step of registration is to find a best match between the reference sample segment image and the search area.

The last step is performed on a digital computer by comparing the two images. The current scheme[3] uses the edge images obtained from the original gray level images. First, an edge detection algorithm using a 3-by-3 area is applied and gray level images are converted into binary images where edge pixels are represented by 1's and the others (or non-edge points) by 0's. Let us call the first acquired image the reference image and the second the input image, which is larger in size. The binary image corresponding to the reference image is placed on the other binary image. All the possible locations are then tried exhaustively by shifting the smaller size binary reference image vertically and horizontally (or along the pixel and scan line direction). At each location the correlation is measured by the number of 1's which coincide and normalized by the total number of 1's. The maximum correlation among the combinations defines the position of best match or registration location.

The problem of image registration is well known. Bernstein developed techniques for precise geometric correction of LANDSAT data[5,6]. These techniques involve the modelling of all geometric errors. The ground control point location is used to determine the image external geometry. Both sequential similarity detection algorithms (SSDA)[7] and conventional correlation methods (e.g., FFT) have been used. By fitting a correlation surface to the registration results, Bernstein has achieved subpicture element accuracy. These registration techniques initially require manual selection of ground landmarks such as highways and airports. Thereafter, the registration operation is automatic. For the application with which we are concerned, images are primarily agricultural and the accuracy of registration that we require is better than one-half picture element (pixel).

The approach presented here is to set up 60 small overlapping subimages in each of two images at prescribed locations. Correlation is then performed on these subimage pairs all using a normalized version of an SSDA with which scenic change due to crop phenology is better handled. The resulting 60 similarity matrices are examined for sharpness and the consistency of computed shifts (Δx_i, Δy_i) is examined. The final result is a best-fit shift (Δx, Δy). A statistical measure of these shifts constitute the analysis of registration accuracy.

Registration Using Normalized Sequential Similarity Detection Algorithm

One of the most important considerations in developing a registration checking algorithm for LACIE is that the image pairs are usually in nearly perfect registration. Our task is therefore to search for a best match within a small range, say plus and minus 5 pixels.

Both images, which are called a reference and an input image, are LACIE images of 196 pixels-by-117 lines. They are, of course, acquired on different dates and therefore the two satellite positions may be different. Possible sources of geometrical differences in two images are

- shifts along the x axis (the pixel direction) and/or y axis (the line direction,)
- rotation,
- stretch, and
- shearing.

These transforms are illustrated in Figure 1.

It should be noted that as a result of resampling performed before registration the magnitude of the above errors is small. It is expected that the rotation error should be within one degree and the stretch error not exceed one per cent.

It is not feasible to consider all the above transforms to find the best match because the number of possible combinations is too large. An alternative is first to register the small subimage pairs extracted from the two images. For each subimage pair, a best match is determined solely by shifting along the x and y coordinates. For small subimages the dominant transform is the x and y shift. For example, a one per cent stretch error and one degree rotation error produces approximately a 2 pixel and a 3 pixel distortion, respectively, on a

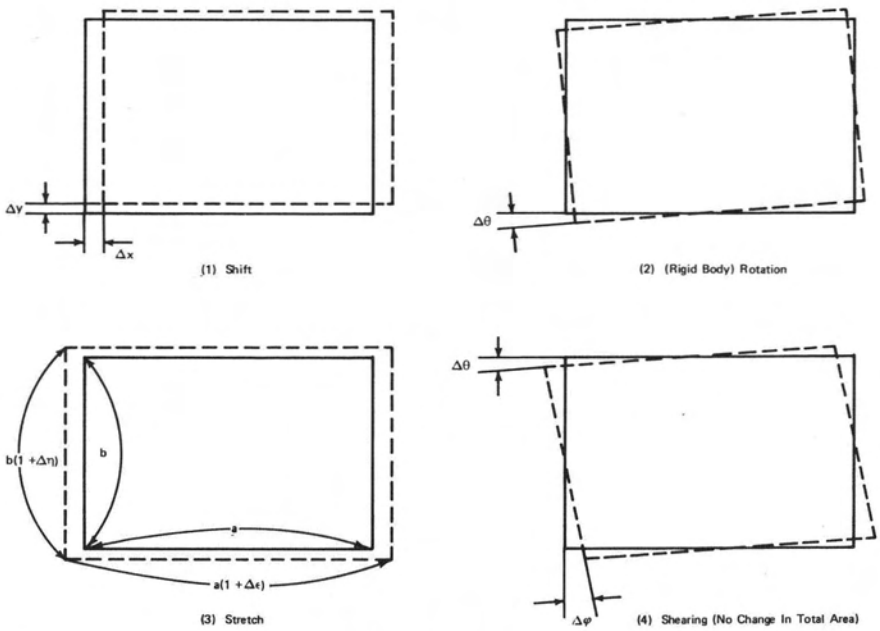

FIG. 1. Four linear transforms.

196-by-117-image, but only 0.2 and 0.3 pixels on an image of one-tenth of this size. In the computer program described in this paper, we set up 60 subimage or window pairs of 27 pixels-by-27 scan lines and 39 pixels-by-39 scan lines as are shown in Figures 2(a) and 2(b). Correlation is then performed on each of these subimage pairs. A best match is found which provides the shifts needed to bring each of the pairs in registration. A six-parameter transform from the (x,y) coordinate system to a new coordinate system (p,q) is calculated, for computed local shifts Δx_i and Δy_i of the i th window pair whose center is located at (x_i, y_i).

$$\begin{aligned} p &= ax + by + c \\ q &= dx + ey + f \end{aligned} \tag{1}$$

The six coefficients are determined under the least squares criteria,

$$\underset{a,b,c,d,e,f}{\text{Min}} \quad \sum_{i=1}^{N} \left\{ (p_i - ax_i - by_i - c)^2 + (q_i - dx_i - ey_i - f)^2 \right\}$$

where N is the number of window pairs, $p_i = x_i + \Delta x_i$, and $q_i = y_i + \Delta y_i$.

With this approach there is a need for a technique which will rapidly correlate two small subimages. It was found that methods using edges did not perform well on the small subimages being used.

We chose to work with gray level images rather than edge images by using a sequential similarity detection algorithm (SSDA) similar to the one developed by Barnea and Silverman[7]. Our modification of SSDA can be called a normalized SSDA. An SSDA is a very fast computing method. It is generally two orders of magnitude faster than the direct correlation using the fast Fourier transform. SSDA and fast Fourier Transform methods have been successfully employed by Bernstein[5,6] to automatically locate control points used to correct and register LANDSAT images.

Generally speaking, SSDA's may be divided into two categories: constant threshold SSDA's and adaptive threshold SSDA's. The latter are potentially faster than the former, but more difficult to implement. We selected a constant threshold SSDA. The following sketches a constant threshold SSDA.

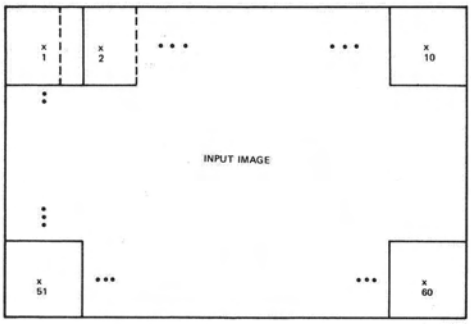

FIG. 2. (a) Sixty subimages on an input image.

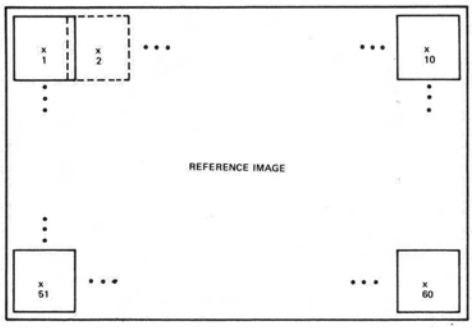

FIG. 2. (b) Sixty subimages on a reference image.

Let a larger (L pixel-by-L-scan line) subimage from the input image be called a search subimage and a smaller (M pixel by M scan line) subimage from the reference image be called a window subimage. They are represented by two arrays, respectively,

$$\begin{matrix}\{R(i,j)\} & 1 \leq i, j \leq L, & \text{and} \\ \{W(k,m)\} & 1 \leq k, m \leq M. & \end{matrix}$$

There are $(L - M + 1)^2$ possible locations to check by vertically and horizontally shifting the window subimage on the search subimage. Consider a position, illustrated in Figure 3, where the (1,1) element of the window subimage is placed on the (I,J) element of the search subimage. Let $R^{I,J}(k,m)$ denote the M by M subimage of the L by L search subimage directly underneath the M by M window subimage. The total sum of the absolute differences,

$$E(I,J) = \sum \left| R^{I,J}(k,m) - W(k,m) \right| \qquad 1 \leq k, m \leq M,$$

is a measure of their correlation. The best match is identified by the (I, J) pair which yields the smallest sum. A time saving idea within SSDA's is to halt the computation of this sum whenever the current sum exceeds a threshold. The coordinates of pixel pairs are selected in a non-recurring random manner and the similarity measure is the number of pixel pairs required to make the sum exceed the preset threshold. Let the coordinate of the n th pixel pair be denoted by (k_n, m_n), and the threshold by T. Then the similarity measure $S(I, J)$ of two subimages at the (I, J) shift position is given by

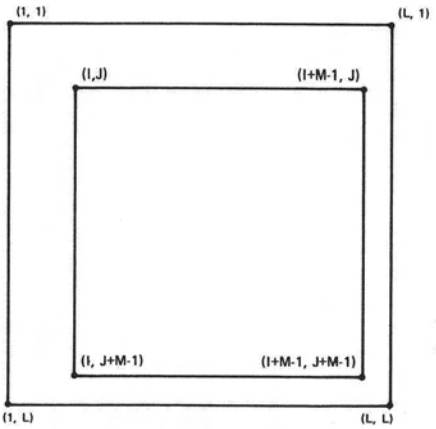

FIG. 3. An M by M window subimage placed on the corresponding L by L search area.

$$S(I, J) = r \text{ such that}$$

$$\sum_{n=1}^{r+1} |D(k_n, m_n)| \geq T, \text{ and}$$

$$\sum_{i=1}^{r} |D(k_n, m_n)| < T, \tag{2}$$

where

$$D(k_n, m_n) = R^{I,J}(k_n, m_n) - \overline{R}^{I,J} - W(k_n, m_n) + \overline{W},$$

$$\overline{R}^{I,J} = M^{-2} \sum \sum R^{I,J}(i,j) \qquad 1 \leq i, j \leq M, \text{ and}$$

$$\overline{W} = M^{-2} \sum \sum W(i,j) \qquad 1 \leq i, j \leq M .$$

After examining all (I,J) locations, we obtain a similarity matrix of integer number entries $\{S(I,J)\}$, $1 \leq I, J \leq L - M + 1$. The location of the best match is the one which has the largest entry. Consequently, its coordinate (I_o, J_o) gives the horizontal shift (Δx) and vertical shift (Δy) needed to bring the window and search subimage into registration.

NORMALIZED SSDA

The main difficulty in using constant threshold SSDA's is the choice of a threshold value T. If T is small, the number of pixel pairs examined is too small and the resulting similarity matrix $S(I, J)$ is unreliable. If T is too large, the computation time becomes unnecessarily long. It may even occur that the similarity matrix reaches the maximum (i.e., equals the total number of points in the window) at two or more places. The selection of a suitable threshold is often experimental.

When we applied a constant threshold SSDA to our problem, the following two difficulties arose in addition to the above threshold selection problem:

(1) The number of image points r in Equation 2 becomes unnecessarily large whenever both search subimages and window subimages were from uniform areas such as large lakes or large sand dunes. This problem would not arise when reference subimages of easily identifiable landmarks were chosen manually.

(2) Changes in scenic contrast due to crop phenology may preclude well-defined correlation from being found. The second difficulty is inherent to SSDA's use of gray level image values.

It was found that use of a normalized version of the SSDA reduced the above difficulties. With this modification, a similarity matrix $S(I,J)$ is given by

$$S(I,J) = r \text{ such that}$$

$$\sum_{n=1}^{r+1} |D(k_n, m_n)| \geq T, \text{ and}$$

$$\sum_{n=1}^{r} |D(k_n, m_n)| < T, \tag{3}$$

where

$$D(k_n, m_n) = \frac{R^{I,J}(k_n, m_n) - \overline{R}^{I,J}}{\sigma_{I,J}} - \frac{W(k_n, m_n) - \overline{W}}{\sigma_w}$$

$$\sigma_{I,J} = M^{-2} \sum \sum (R^{I,J}(i,j) - \overline{R}^{I,J}), \qquad 1 \leq i, j \leq M$$

$$\sigma_w = M^{-2} \sum \sum (W(i,j) - \overline{W})^2, \qquad 1 \leq i, j \leq M .$$

For the distance measure ($D(k_n, m_n)$ in Equation 2 only the mean level adjustment was performed, which is able to compensate for an additive term.

The normalization compensates for a linear transform of pixel values. More specifically, if linear transforms $av + b$ and $a'v + b'$ (a, a', b, and b' are constant coefficients) are operated on the two images to be registered, the resulting similarity matrices from Equation 3 are unchanged. This normalization scheme permits the same threshold to be used for each of the four channels. Hence, the experimental determination of a suitable threshold is relatively easy with the normalized SSDA.

In fact, if the pixels in both search and window subimages are assumed to be independently and normally distributed, the expected number of pixels used under a threshold T is given by

$$N = 0.5\sqrt{\pi T}$$

and also the standard deviation

$$\sigma_N = \sqrt{0.5(\pi-2)\,\overline{N}}$$

With $T=70$, which we employed in our experiment, we have $\overline{N} \sim 62$ and $\sigma_N \sim 6$. It is noted that the above expressions are dependent only upon the threshold T but not on the standard deviation of the normal distribution. Roughly speaking, if the number of points is larger than $\overline{N}$, then the two subimages are correlated positively and when this number is smaller, the subimages are negatively correlated.

The problem caused by scenic change due to crop phenology cannot be solved by a normalization scheme alone, but its effect is reduced considerably. As long as crop phenology affects the subsequent image in a roughly linear fashion, the resulting similarity matrix will have a well-defined peak. This condition is more likely to occur on a smaller area. When a window area of 27-pixels-by-27 scan lines was employed, it was found that successful correlation was often obtainable even when the considerable non-uniform change could be seen in the entire image of the subsequent acquisition.

Details of Registration Scheme

A general outline of our registration checking algorithm was described earlier. This section will describe its details.

In our experiment 60 subimage pairs were set up as shown in Figures 2(a) and 2(b). The size of a window subimage is 27-by-27 and that of a search subimage is 39-by-39, so that 169 locations accounting for plus-and-minus 6 vertical and horizontal shifts are examined. All these parameters are inputs to the program. The normalized SSDA operation is performed on each of the 60 window and search subimage pairs. This gives 60 similarity matrices, each of which is a 13-by-13 array. Since the subimage pairs were set up automatically, some of them will not correlate well. For example, a subimage containing a straight road is not a good feature for registration whereas an intersection is. Each of the resulting similarity matrices is examined for its sharpness of the correlation peak. The location of the peak yields the shift (Δx_i) along the x-axis and shift (Δy_i) along the y-axis which is needed to bring the i th subimage pair into registration. The second test is then performed for the shift pairs that passed the first test for consistency with each other. The details of these tests are described in the following subsections a and b.

SHARPNESS OF CORRELATION

The sharpness-of-correlation test is

(1) The maximum number v_0 of a similarity matrix $\{S(I,J)\}$, $I,J = 1,2, \ldots, 13$ is found and its coordinate (I_0,J_0) yields the shift pair $(\Delta x_i, \Delta y_i)$. Explicitly we have $\Delta x_i = I_0 - 7$ and $\Delta y_i = J_0 - 7$.

(2) Six circles are drawn around (I_0, J_0) as
$(I-I_0)^2 + (J - J_0)^2 \leq r^2$, $r = 1, 2, 3, 4, 5$, and 6.

(3) Inside each ring the maximum number is computed.
$$v_i = \{\text{Max } S(I,J) \mid (i-1)^2 < (I-I_0)^2 + (J-J_0)^2 \leq i^2\} \quad (4)$$

(4) Also the maximum number outside the largest circle is computed,
$$v_7 = \{\text{Max } S(I,J) \mid (I-I_0)^2 + (J-J_0)^2 > 36\} \cdot \quad (5)$$

The decision concerning whether or not the resulting similarity matrix is useful is based upon the eight values $v_0, v_1, \ldots, v_7$. Since $v_0 \geq v_1, v_2, \ldots, v_7$, let $u_i = v_0 - v_i$, $i = 1,2, \ldots,7$, and $u_a = (u_4 + u_5 + u_6)/3$. The conditions to be imposed are

(1) $u_a/v_0 \geq 0.15$
(2) $u_2 \geq 0.1\, u_a$
(3) $u_3 \geq 0.2\, u_a$
(4) $u_4 \geq (u_5 + u_6)/2$, $u_5 \geq (u_4 + u_6)/2$, $u_6 \geq |(u_4 + u_5)/2$
(5) $u_7 \geq 0.5\, u_a$

In most of the cases the values of u_1, u_2, and u_3 are increasing in this order but those of u_4, u_5, and u_6 are more or less similar. So the ratio u_a/v_0 describes the sharpness of the peak in comparison with its surroundings. The second and third conditions are on its slope. Note here that no conditions are placed upon the u_1 so that $u_1 = 0$ or $v_0 = v_1$ is acceptable. Condition 5 says that the secondary peak should not exceed the mean value of v_0 and $(v_4 + v_5 + v_6)/3$.

CONSISTENCY TEST

The second test is carried out on the shift pair $(\Delta x_i, \Delta y_i)$ that passed the first test. Some of the pairs may be inconsistent in comparison with the rest. An iterative procedure is used to identify and eliminate inconsistent shifts. We begin by computing six parameters in Equation 1 calculated with all the eligible shifts pairs $(\Delta x_i, \Delta y_i)$. The error is defined by

$$e_i = \sqrt{(\Delta x_i - \Delta \hat{x}_i)^2 + (\Delta y_i - \Delta \hat{y}_i)^2}$$

where $\Delta \hat{x}_i = ax_i + by_i + c - x_i$ and $\Delta \hat{y}_i = dx_i + ey_i + f - y_i$ are the first estimate of shift pair. If $e_i > 3$, then the pair $(\Delta x_i, \Delta y_i)$ is discarded. Then the second iteration is carried out with the remaining pairs. Once more the error is calculated and a stricter condition $e_i > 2.5$ is used to eliminate inconsistant shifts. A final iteration is performed using the condition $e_i > 2$. The resulting six parameters constitute the final answer.

The following subsection will describe the derivation of the best-fit shifts, and the rotation angle and stretch factors from the resulting six parameters. The next subsection will be concerned with the reliability of these results.

GEOMETRICAL INTERPRETATION

Equation 1 can be rewritten as

$$\begin{aligned} p &= a(x - \Delta x) + b(y - \Delta y) \\ q &= d(x - \Delta x) + e(y - \Delta y) \end{aligned} \tag{6}$$

where

$$\begin{aligned} a\Delta x + b\Delta y &= c, \text{ and} \\ d\Delta x + e\Delta y &= f. \end{aligned} \tag{7}$$

The pair $(\Delta x, \Delta y)$ is the best-fit shift from the (x,y) coordinate system to the (p, q) system. Let $x - \Delta x = X$ and $y - \Delta y = Y$. Then Equation 6 can be written as

$$\begin{aligned} X &= Ap + Bq \\ Y &= Cp + Dq \end{aligned}$$

The angles from X-axis to p-axis and from Y-axis to q-axis (see Figure 4) are

$$\begin{aligned} \theta_p &= \tan^{-1}(C/A) \\ \theta_q &= \tan^{-1}(B/D) \end{aligned} \tag{8}$$

The stretching factors are, respectively,

$$\begin{aligned} t_p &= \sqrt{A^2 + C^2} \\ t_q &= \sqrt{B^2 + D^2} \end{aligned} \tag{9}$$

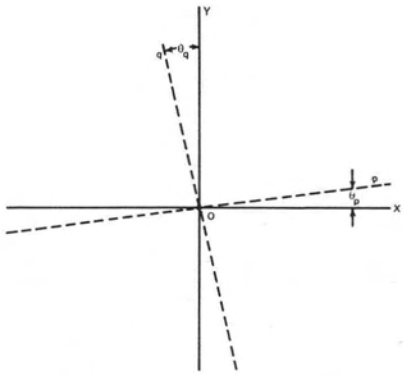

FIG. 4. Geometrical relationship between the *(X,Y)* and *(p,q)* coordinate system.

RELIABLE REGISTRATION

To determine six linear coefficients in Equation 1, we need at least three pairs of shifts $(\Delta x_i, \Delta y_i)$. Generally, the larger the number of shift pairs used in the final answer, the more reliable are the coefficients. A tentative criteria is nine pairs. That is, if the total number of shifts pairs surviving with both screening tests is less than or equal to nine, we say that the registration result for the image pair concerned should not be trusted. It has been found that this condition generally occurs in two cases: (1) at least one image is of low quality due to clouds or haze, or (2) the two images look different probably due to crop phenology.

EXPERIMENTS AND DISCUSSIONS

A computer program for our registration checking algorithm was written in FORTRAN IV and executed in an IBM 360/75. Experiments were carried out for 44 LACIE sample segments, each of which had four acquisitions. Registration was checked on all the six combinations per sample segment, that is, acquisition 1 with acquisition 2, 1 with 3, 1 with 4, 2 with 3, 2 with 4, and 3 with 4. Approximate CPU time was three-minutes-and-a-half for all six checks when a threshold of 70 was employed. The total number of registration checks is 264 (6-by-44).

An example of LACIE image sets is shown in Figures 5(a), (b), (c), and (d). They are all from channel 2 (0.6 to 0.7 μm). They were acquired on October 19, 1974, May 14, June 19, and July 7, 1975, respectively. These dates correspond to four biological phases of wheat development at the location: pre-emergence, green, mature, and post-harvest. On each of the images, identical training fields are superimposed. The work of defining these fields was performed based on the fourth acquisition, Figure 5(d). Misregistration of these fields on the other images is evident. The best fit shifts $(\Delta x, \Delta y)$ computed by our computer program are $(-1.48, -0.12)$, $(-1.57, 0.26)$, $(-1.45, -0.01)$, $(-0.03, 0.70)$, $(0.06, 0.05)$, and $(-0.21, -0.37)$ between acquisition 1 with 2, 1 with 3, 1 with 4, 2 with 3, 2 with 4, and 3 with 4, respectively. the numbers of surviving pairs with two screening tests are 32, 42, 41, 43, 44, and 42, respectively. These shifts agree well with a visual inspection of the imagery, although an accurate check is difficult.

The details of our scheme for a given pair of acquisitions can be illustrated using Figure 5(a) as the reference image and Figure 5(b) as the input image. Table 1 gives a summary of the results of 60 subimage pair correlations performed by our program. The first two columns describe the x and y coordinate of the center of each subimage pair. The next two columns *(DX* and *DY)* are the computed shifts between the two subimages. The fifth column shows the maximum number v_0 of a similarity matrix. The next seven numbers are $(v_0 - v_i)$, $i = 1,2, \ldots, 7$, where v_i's are defined in Equations 4 and 5. The computed shifts in Columns 3 and 4 are illustrated in Figure 6. The + signs designate the center of subimage pairs and the * signs the result of shifts. Only the correlated pairs surviving the sharpness test are plotted on the map. Those pairs eliminated by the consistency test are indicated by arrows.

FIG. 5. (a) A LACIE sample segment acquired on October 19, 1974.

FIG. 5 (b) The image of the same sample segment on May 14, 1975.

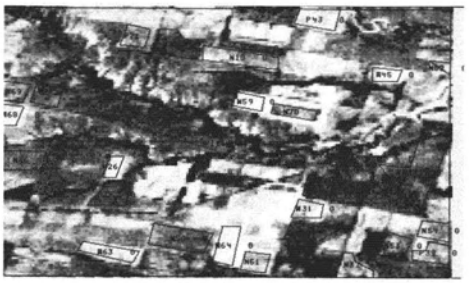

FIG. 5 (c) The image of the same sample segment on June 19, 1975.

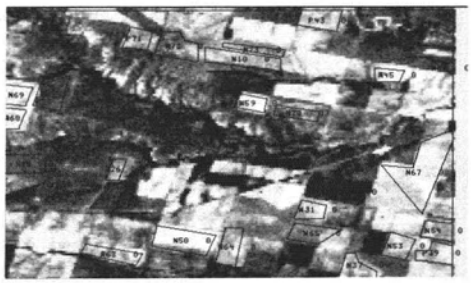

FIG. 5. (d) The image of the same sample segment on July 7, 1975.

For this pair of images, the best-fit linear transformation calculated from the 36 surviving shift pairs $(\Delta x_i, \Delta y_i)$ was

$$p = 0.998x - 0.002y - 1.476$$
$$q = 0.005x + 0.996y - 0.120$$

From Equation 7 we have the best fit shift pair

$\Delta x = -1.482$ and $\Delta y = -0.125$

The rotation angles $\theta_p = -0.259$ degree and $\theta_q = -0.131$ degree are derived from Equation 8, where the positive direction is counter clockwise. The stretch factors $t_p = 1.002$ and $t_q = 1.004$ are obtained from Equation 9.

The same calculation was performed for each of 264 registration checks. For presentation of these results, we restrict ourselves only to be best fit shift results, because the LACIE image size (196 pixels-by-117 scan lines) is too small to determine possible small angle rotations and stretch factors reliably. (For this purpose full-frame LANDSAT images are to be used.) Furthermore, when best-fit shifts are rounded to the nearest integers, they can be used for re-registration without a resampling operation (that is, shift-only).

When the total 264 registration checks were carried out using channel 2, 68 were judged to be unreliable because the number of subimage pairs surviving the sharpness and the consistency test was less than or equal to 9. The average number of surviving pairs was 33.5. Among these 68 checks 30 were caused by poor image quality due to cloud or haze. The remaining 38 were due to scene change. Hence, the failure rate of the algorithm was 38/235 (16.2 per cent). Histograms for best-fit shifts Δx and Δy and their root square value $\sqrt{(\Delta x)^2 + (\Delta y)^2}$ are shown in Figures 7(a), (b), and (c), respectively, where 0.1 pixel quantization is employed. It can be observed that the ranges of Δx and Δy are restricted within plus/minus 2 pixel and plus/minus 1 pixel, respectively. One reason for the observation that the distribution of Δx is wider than that of Δy is that the LANDSAT images are less sharp and edges are less reliable along the x axis (the pixel direction) due to the fact that the LANDSAT multispectral sensor has approximately a 30 per cent overlap in the field of view along the pixel direction. From Figure 7(c) we find the probability $\sqrt{(\Delta x)^2 + (\Delta y)^2} \leq 1.0$ is 0.69. The root-mean-square of $\sqrt{(\Delta x)^2 + (\Delta y)^2}$ is 0.99 pixel, which satisfies the target of the current

TABLE 1. A SUMMARY OF THE RESULTS OF SIXTY SUBIMAGE PAIR CORRELATIONS BETWEEN FIGURE 5(a) AND 5(b).

X	Y	DX	DY	Max	1	2	3	4	5	6	Max Outside
20	20	−2	−1	106	2	9	16	18	21	25	25
37	20	−2	0	114	1	6	8	13	10	19	22
54	20	−3	0	77	4	5	6	9	5	8	0
71	20	−2	0	88	6	9	9	10	10	10	10
89	20	−4	−6	84	2	4	4	4	11	5	5
106	20	−5	4	101	12	12	5	0	8	5	0
123	20	5	−2	85	1	6	9	9	9	10	8
141	20	−2	1	103	1	8	12	13	18	20	15
158	20	−2	0	116	0	17	24	25	37	39	34
175	20	0	5	83	2	2	2	4	2	12	12
20	35	−1	0	170	3	9	31	32	40	48	46
37	35	−4	0	135	0	0	1	8	16	21	17
54	35	−1	−1	117	1	22	27	26	28	30	30
71	35	−2	0	93	2	0	10	5	12	11	12
89	35	−3	0	91	2	2	13	15	16	18	18
106	35	0	1	77	0	2	4	7	5	7	4
123	35	1	0	90	1	6	7	12	16	26	23
141	35	−1	0	104	2	7	6	9	6	14	16
158	35	−3	0	110	8	2	5	11	33	31	25
175	35	4	−2	84	3	4	13	13	17	11	3
20	50	0	0	122	1	18	18	25	28	29	41
37	50	−2	−1	121	0	7	15	10	29	31	33
54	50	−1	0	158	23	46	54	61	67	67	75
71	50	0	1	126	5	17	17	35	33	34	36
89	50	2	2	93	2	4	3	7	10	12	14
106	50	0	−1	120	7	19	27	31	36	27	55
123	50	−1	0	126	15	34	37	44	47	49	48
141	50	−2	0	101	3	9	10	16	19	19	18
158	50	−1	0	117	2	14	23	30	31	32	41
175	50	1	1	111	4	1	3	2	11	20	23
20	66	−1	0	166	17	44	49	57	60	62	69
37	66	0	0	127	6	22	25	30	23	29	30
54	66	−2	0	99	0	2	3	5	5	8	20
71	66	−2	0	128	7	25	34	34	38	48	40
89	66	−2	0	122	11	19	24	28	34	37	36
106	66	−2	0	123	5	6	14	16	24	25	19
123	66	−2	0	123	7	20	16	12	38	32	34
141	66	−2	0	102	5	11	20	21	23	27	33
158	66	−1	0	100	3	17	28	28	32	37	39
175	66	−1	0	117	2	10	17	20	24	23	24
20	81	−1	−1	148	17	18	29	26	45	49	57
37	81	−2	0	133	12	30	40	37	39	39	36
54	81	−1	0	144	8	41	45	44	47	45	48
71	81	−2	0	132	6	31	35	31	40	40	43
89	81	−1	0	118	1	18	29	16	40	41	43
106	81	0	−1	126	8	11	28	25	29	30	36
123	81	0	0	95	1	1	9	4	9	15	21
141	81	−2	−1	117	0	8	8	8	13	18	17
158	81	−1	0	139	3	3	15	16	42	42	45
175	81	−1	0	134	1	14	29	37	39	52	53
20	96	−2	−1	129	1	22	36	38	43	46	50
37	96	−1	−1	133	7	35	37	37	48	47	50
54	96	−2	−1	108	0	18	21	26	29	28	27
71	96	−1	0	103	6	9	11	9	13	11	19
89	96	1	−2	94	9	7	1	4	7	6	6
106	96	−2	0	112	9	10	15	17	27	30	28
123	96	−2	0	135	2	25	32	31	42	40	40
141	96	−1	0	138	8	15	25	34	44	58	58
158	96	−2	0	170	27	30	44	46	46	54	54
175	96	−2	0	162	1	18	23	30	42	41	42

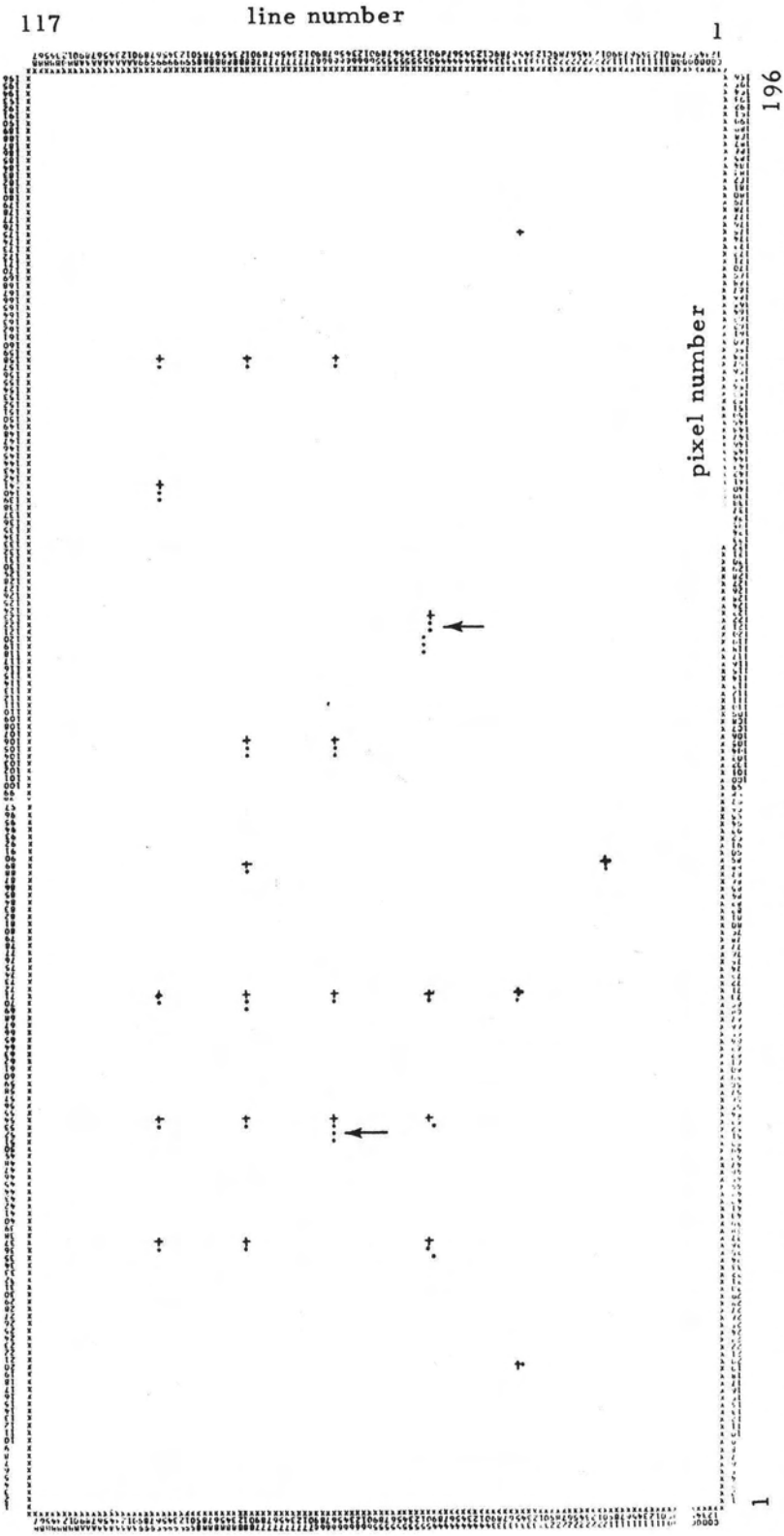

FIG. 6 The map showing the calculated shifts between subimage pairs surviving the sharpness test. The pairs eliminated by the consistency test are indicated by arrows.

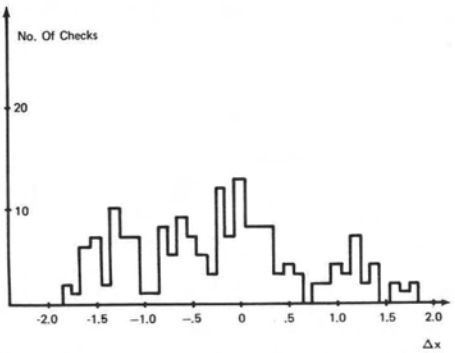

FIG. 7. (a) Histogram of best fit shifts Δx using channel 2.

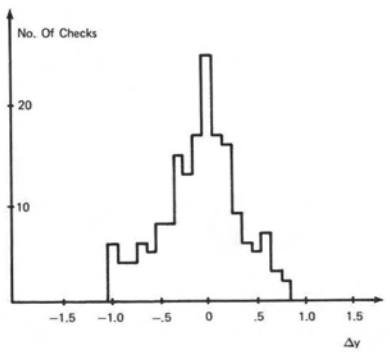

FIG. 7. (b) Histogram of best fit shifts Δy using channel 2.

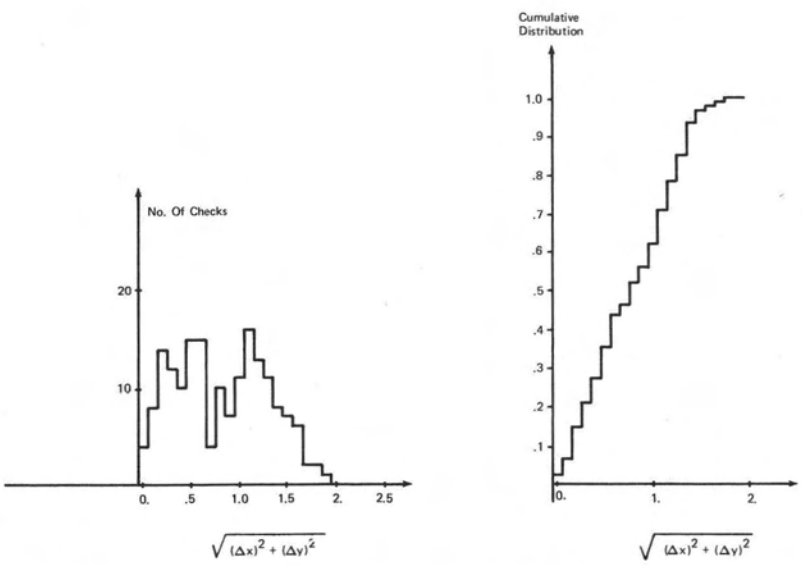

FIG. 7. (c) Histograms of root square $(\Delta x^2 + (\Delta y)^2$ using channel 2.

registration procedure 1.0 pixel. Table 2 (a) shows the distribution of calculated shifts (Δx, Δy) which were rounded off to the nearest integer. These rounded pairs may be used for re-registration.

An important question concerns how accurately the presented registration check scheme can compute misregistration. Since there is no misregistration truth known for the data set we used, this question is not easy to answer. An attempt was made to check visually by using the imagery itself. However, the accuracy was disappointingly low (probably poorer than 0.5 pixel). Seven of the sample segments with one or more pixel misregistrations were checked by a professional photo interpreter with reasonably good agreement.

In another attempt to estimate the registration checking scheme, we repeated the program execution by using channel 4. When channel 4 was used, 70 checks were judged to be unreliable among 264. The average number of surviving subimage pairs was 34.4. Among these 70 checks, 30 were caused by the fact that one or both images are of poor quality due to cloud or haze. Therefore, the failure rate is 40/234 (17.1 per cent). Although this agrees with the results from channel 2, we observed that the instances where registration checking failed on both channel 2 and channel 4 due to scene change was only 19 among 234 (8 per cent). Figure 8(a), (b), and (c) shows histograms for best fit shifts Δx and Δy and their root square, $\sqrt{(\Delta x)^2 + (\Delta y)^2}$, respectively, using channel 4. All these histograms closely resemble those

TABLE 2(a). THE DISTRIBUTION OF ROUNDED BEST FIT SHIFTS USING CHANNEL 2.

DY \ DX	−2	−1	0	1	2
−1	0	13	16	5	2
0	8	46	58	24	4
1	1	3	6	7	1

TABLE 2(b). THE DISTRIBUTION OF ROUNDED BEST FIT SHIFTS USING CHANNEL 4.

DY \ DX	−2	−1	0	1	1
−1	1	10	13	6	2
0	11	54	60	19	2
1	1	4	6	4	1

obtained using channel 2. The root mean square, $\sqrt{(\Delta x)^2 + (\Delta y)^2}$, is 1.0 pixel which is exactly the same as the target of the current registration procedures. The rounded best-fit shifts (Δx, Δy) are shown in Table 2(b).

To compare the results from channel 2 and channel 4, we calculate statistics of the differences

$E_x = \Delta x$ of channel 2 $- \Delta x$ of channel 4.
$E_y = \Delta y$ of channel 2 $- \Delta y$ of channel 4.

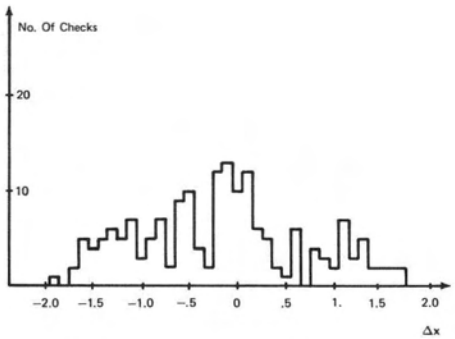

FIG. 8. (a) Histogram of best fit shifts Δx using channel 4.

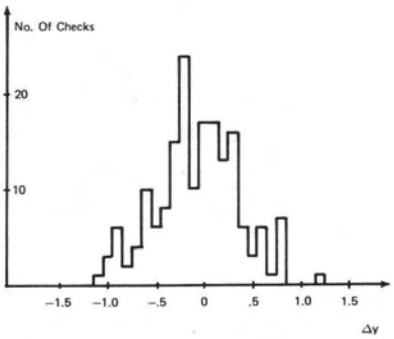

FIG. 8. (b) Histogram of best fit shifts Δy using channel 4.

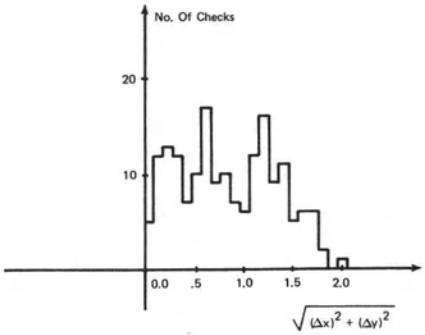

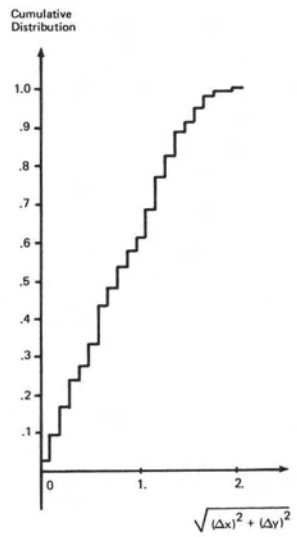

FIG. 8. (c) Histogram of root squares $(\Delta x)^2 + (\Delta y)^2$ using channel 4.

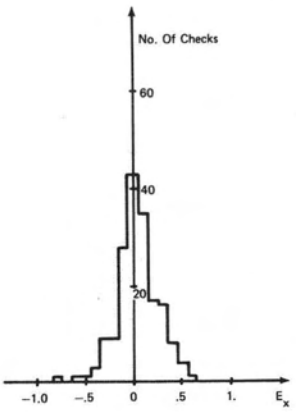

FIG. 9. (a) Histogram of E_x.

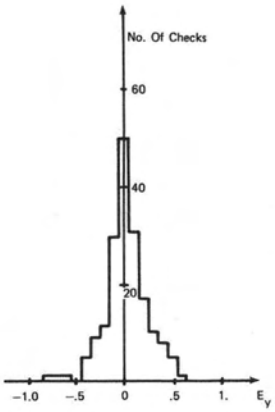

FIG. 9. (b) Histogram of E_y.

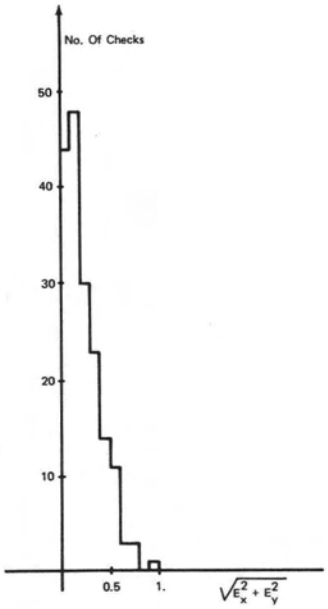

FIG. 9. (c) Histogram of $\sqrt{E_x^2 + E_y^2}$.

Figure 9(a), (b), and (c) show the histograms of E_x, E_y and $\sqrt{E_x^2 + E_y^2}$, respectively, with 0.1 pixel quantization. It is to be noted that the differences E_x and E_y include the errors from both the channel 2 and channel 4 results. From these histograms we may come to a conservative conclusion that the standard deviation of the results obtained by our registration checking algorithm is less than or equal to 0.2 pixel.

Looking at Figure 9(a) and 9(b) we see that there are some cases for errors E_x or E_y exceeding 0.5 pixel. For such cases it was found that areas for which best-fit shift pairs (Δx_i, Δy_i) are obtained give considerably different results between channel 2 and channel 4. For instance, consider an image pair in which misregistration is 1 pixel at the extreme left side and decreases to zero at the right edge. If channel 2 picks up good registration landmarks primarily in the left side area, we will get misregistration close to 1. On the other hand, if good registration landmarks are picked up on the right side area with channel 4, the misregistration will be close to 0, resulting in a large E_x.

ACKNOWLEDGMENTS

The author acknowledges Dr. J. Engvall and Dr. Q. A. Holmes, Johnson Space Center, National Aeronautics and Space Administration, for encouragement, enthusiasm, and helpful discussions throughout this work, and Mr. S. G. Wheeler, his colleague, for providing the statistical calculations used in the section "Details of Registration Scheme." Special thanks are due to Dr. Holmes for reading the initial manuscript. This work was supported by Johnson Space Center, NASA, under Contract No. NAS 9-14350.

REFERENCES

1. R. B. MacDonald, F. G. Hall, and R. B. Erb, "The Use of LANDSAT Data in a Large Area Crop Inventory Experiment (LACIE)", *Proc.* of Symposium on Machine Classification of Remotely Sensed Data, Laboratory for Applications of Remote Sensing, Purdue University, West Lafayette, Indiana, pp 1B-1, June 3, 1975.
2. J. A. Quirein and M. C. Trichel, "Acreage Estimation, Feature Selection, and Signature Extension Dependent upon the Maximum Likelihood Decision Rule," *ibid,* pp 2A-26.
3. M. L. Nack, *Interim Report on Temporal Registration of Multispectral Digital Satellite Images Using Their Edge Images,* Contract NAS5-11999, NASA, Goddard Space Flight Center, Greenbelt, Maryland, April 1975.
4. G. Nagy, "Digital Images Processing Activities in Remote Sensing for Earth Resources", *Proc's of IEEE,* Oct. 1972, pp 1177-1200.
5. R. Bernstein, *All-Digital Precision Processing of ERTS Images,* Contract NAS5-21716, NASA, Goddard Space Flight Center, Greenbelt, Maryland, April 1975.
6. R. Bernstein, "Digital Image Processing of Earth Observation Sensor Data", *IBM Journal of Research and Development,* Vol. 20, No. 1, Jan 1976.
7. D. I. Barnea and H. F. Silverman, "A Class of Algorithms for Fast Digital Image Registration", *IEEE Tr. On Computers,* February 1972, pp 179-186.